RSC Medicinal Chemistry

ROYAL SOCIETY OF CHEMISTRY

RESEARCH ARTICLE

Cite this: *RSC Med. Chem.*, 2024, **15**, 3212

Inhibiting SARS-CoV-2 viral entry by targeting spike:ACE2 interaction with *O*-modified quercetin derivatives†

Reuben James Z. Rosal and Monissa C. Paderes *

The cell entry of severe acute respiratory syndrome coronavirus 2 (SARS-CoV-2) is mediated by the interaction between the receptor-binding domain of its spike (S) protein and human angiotensin-converting enzyme 2 (ACE2). Quercetin, a flavonoid found abundantly in plants, shows potential as a SARS-CoV-2 S:ACE2 inhibitor but is known to have low bioavailability. Modification of quercetin by capping its hydroxyl moieties could enhance the metabolic stability, solubility, and bioavailability, and reduce toxicity. In this study, sixteen (16) *O*-modified quercetin derivatives were synthesized by incorporating alkyl and acyl moieties of varying lengths, sizes, and polarities to the hydroxyl groups. The SARS-CoV-2 S:ACE2 inhibitory activity and toxicity of the synthesized derivatives were assessed *in vitro*, and their physicochemical properties, pharmacokinetics, and drug-likeness were predicted and evaluated using the SwissADME web tool. Results showed that functionalization of the hydroxyl moieties of quercetin generally resulted in more potent inhibitors (>50% inhibition). Five (5) derivatives displayed a dose-dependent inhibition against the SARS-CoV-2 S:ACE2 interaction with promising IC_{50} values (*i.e.*, **2e** (IC_{50} = 7.52 μM), **3a** (IC_{50} = 5.00 μM), **3b** (IC_{50} = 25.70 μM), **3c** (IC_{50} = 2.22 μM), and **4b** (IC_{50} = 3.28 μM)). Moreover, these compounds exhibited low hepato-, nephro-, and cardiotoxicity, and their SwissADME profiles indicated favorable physicochemical, pharmacokinetic, and drug-like properties, suggesting their potential as promising lead SARS-CoV-2 S:ACE2 inhibitors.

Received 21st April 2024,
Accepted 16th July 2024

DOI: 10.1039/d4md00286e

rsc.li/medchem

Introduction

In December 2019, a series of unprecedented pneumonia outbreaks were identified in a local seafood market of Wuhan, Hubei Province, China.[1] The outbreak manifested as a range of respiratory tract issues, with mild to severe symptoms that include fever, dry cough, pneumonia, nausea, and respiratory failure.[2] The World Health Organization (WHO) named this illness as coronavirus disease 2019 (COVID-19) and it was determined to be caused by severe acute respiratory syndrome coronavirus 2 (SARS-CoV-2).[3] It was declared a pandemic by March 2020, with over 774 million confirmed cases and more than 7 million deaths as of March 2024.[4]

SARS-CoV-2 belongs to the *Betacoronavirus* genus, along with severe acute respiratory syndrome coronavirus (SARS-CoV) and the Middle East respiratory coronavirus (MERS-CoV), both responsible for major pandemics in November 2002 and April 2012, respectively. Coronaviruses enter the host cells by binding to cell surface receptors, followed by entry into endosomes and subsequent fusion of viral and lysosomal membranes.[5,6] SARS-CoV-2 cell entry is facilitated by the interaction of the transmembrane spike (S) glycoprotein and the human angiotensin-converting enzyme 2 (ACE2) cell receptor.[7,8] This activates membrane fusion between the virus and the host cell, allowing viral RNA to be released into the cytoplasm and establish infection. SARS-CoV-2 S:ACE2 interaction is the pivotal determinant for SARS-CoV-2 infecting a host species thus, targeting this interaction is a promising approach to combat SARS-CoV-2 infection.

Natural products, such as flavonoids, exhibit diverse bioactive properties and have found wide applications in the development and treatment of various diseases.[9–13] Quercetin, a flavonol found in some berries and herbs in high amounts[14] has been identified as one of the most promising antiviral agents, specifically against coronaviruses.[15–17] Based on *in silico* modeling, quercetin is capable of disrupting the early infection process by targeting the interaction between SARS-CoV-2 viral spike protein and ACE2.[18–22] Surface plasmon resonance (SPR) studies further revealed that quercetin has high binding affinities with SARS-CoV-2 S protein and ACE2 receptor, as indicated by the observed low dissociation constants.[23–25] While quercetin

Institute of Chemistry, College of Science, University of the Philippines Diliman, Quezon City 1101, Philippines. E-mail: mcpaderes1@up.edu.ph

† Electronic supplementary information (ESI) available. See DOI: https://doi.org/10.1039/d4md00286e

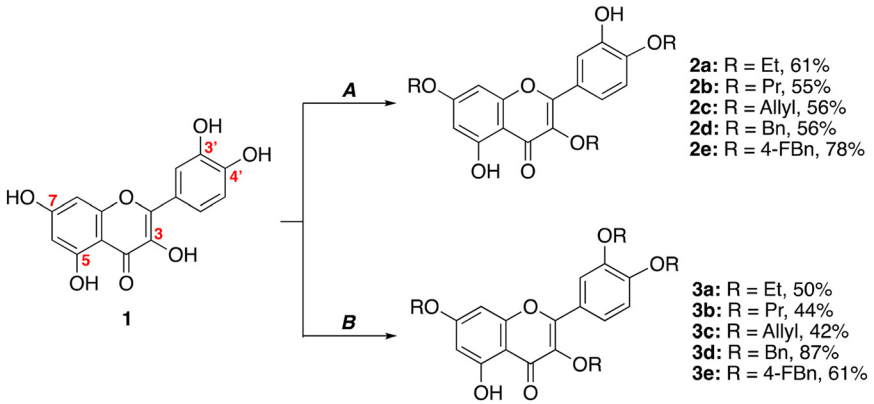

Scheme 1 Synthetic pathway to *O*-alkyl quercetin derivatives. Reagents and conditions: K_2CO_3 (A. 3 equiv. and B. 5 equiv.), RCl/RBr (5 equiv.), DMF, 25 °C, 24 h.

shows potential as a SARS-CoV-2 S:ACE2 blocker, it is also known to have low bioavailability attributed to its low absorption, extensive metabolism, and rapid elimination, making the necessary plasma concentration for effective inhibition insufficient.[14,18,26] Thus, structurally modifying quercetin through capping of its hydroxyl moieties could yield more metabolically stable derivatives with improved solubility and bioavailability, and reduced toxic side effects.[27–29]

In this study, quercetin was derivatized *via* alkylation and acylation of the hydroxyl moieties with substituents of varying length, size, and polarity to determine possible structure–activity relationship (SAR). The derivatives were then evaluated *in vitro* for their inhibitory activity against SARS-CoV-2 S:ACE2 interaction, as well as for hepato-, nephro-, and cardiotoxicity. The physicochemical properties, pharmacokinetics, drug-likeness, and medicinal chemistry friendliness of the derivatives were predicted and assessed using the SwissADME web tool. To the best of our knowledge, this is the first report of the *in vitro* investigation of quercetin derivatives against SARS-CoV-2 S:ACE2 inhibition.

Results and discussion

Synthesis of the *O*-modified quercetin derivatives

The *O*-modification of quercetin *via* alkylation and acylation are summarized in Schemes 1 and 2, respectively, using modified literature procedures.[30,31] The *O*-alkylation of compound **1** with various alkyl halides, utilizing either 3 or 5 equivalents of anhydrous K_2CO_3 in DMF, resulted in *O*-tri- (compounds **2a–e**) and -tetraalkylated (compounds **3a–e**) quercetin derivatives, respectively (Scheme 1). The *O*-alkylated products were obtained in moderate to good yields. In the study reported by Rao and Owoyale, methylation of the hydroxyl groups of quercetin using K_2CO_3 proceeds in a stepwise manner with the following reactivity: $4' > 7 > 3 > 3' > 5$.[32] Similar reactivity trend was observed in this study and by Al-Jabban *et al.* in the synthesis of different *O*-alkyl quercetin derivatives.[30]

O-Acylation reaction was carried out by treatment of compound **1** with 3.5 equivalents of the appropriate acyl chloride and using anhydrous pyridine and CH_2Cl_2 as base and solvent, respectively (Scheme 2). The reaction resulted in a mixture of *O*-tri- (compounds **4a–c**) and -tetraacylated (compounds **5a–c**) quercetin derivatives, which were purified and separated through column chromatography. The poor yields are attributed to the difficult separation of the *O*-tri- and -tetraacylated compounds due to their comparable polarities.

The structures of the *O*-modified quercetin derivatives were confirmed using ^{1}H NMR analysis. For *O*-trialkylated and -triacylated derivatives, the loss of the hydroxyl peaks at positions 3, 4′, and 7 of quercetin and the appearance of the pertinent peaks of the alkyl and acyl groups were monitored. The structures of the *O*-tetraalkylated and -tetraacylated quercetin derivatives, on the other hand, were confirmed by

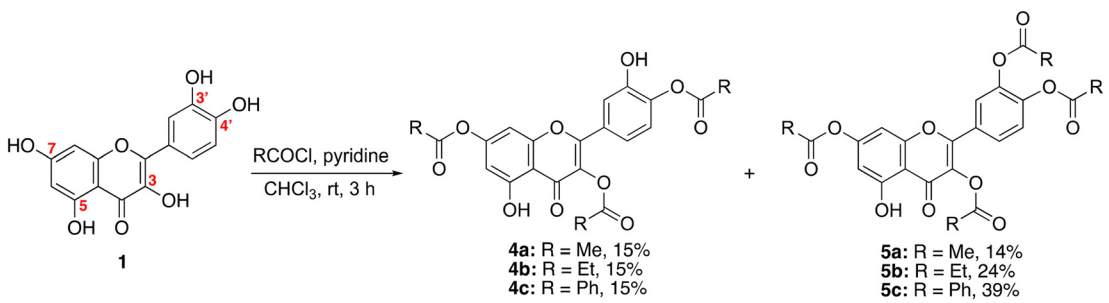

Scheme 2 Synthetic pathway to *O*-acyl quercetin derivatives. Reagents and conditions: acyl halide (3.5 equiv.), pyridine, CH_2Cl_2, 25 °C, 3 h.

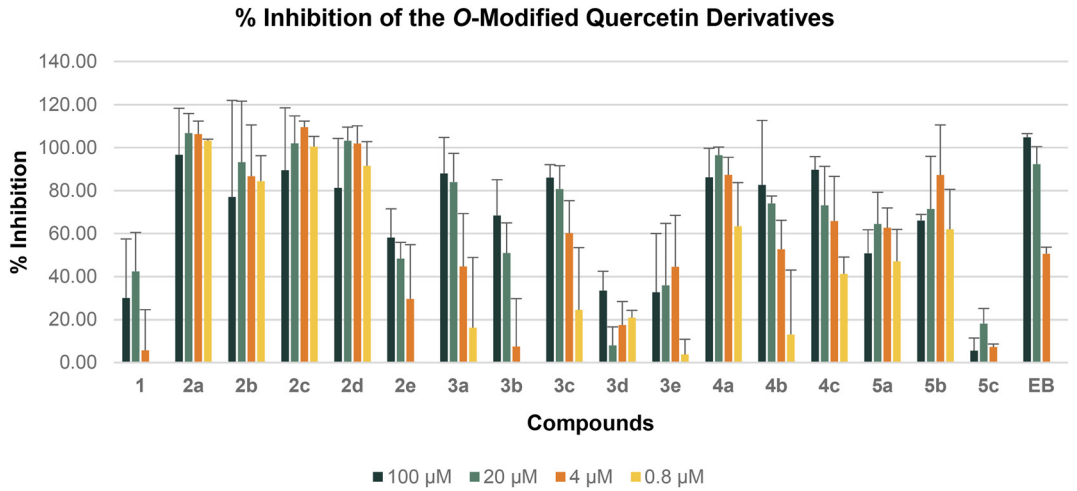

Fig. 1 Summary of the average % inhibition of quercetin (**1**) and the *O*-modified quercetin derivatives in 3 independent trials (n = 3); EB = erythrosine B. The bars depict the standard deviation of the mean (SD).

the disappearance of the 3′ OH peak and the presence of the additional alkyl and acyl peaks. Chemical shifts of the hydroxyl and phenolic groups of quercetin were assigned based on literature values.[30,33] A heteronuclear multiple bond correlation (HMBC) experiment was also conducted on compound **2a** to ascertain the attachment of the ethyl groups to positions 3, 4′, and 7 of quercetin (Fig. S3, ESI†).

In vitro assays of the *O*-modified quercetin derivatives

SARS-CoV-2 spike:ACE2 inhibition assay. The SARS-CoV-2 S:ACE2 inhibition of the synthesized *O*-modified quercetin derivatives was evaluated using a SARS-CoV-2 S_1 receptor binding domain (RBD):ACE2 inhibition assay. This assay employs a colorimetric enzyme-linked immunosorbent assay (ELISA) to screen inhibitors of the ACE2:RBD protein–protein interaction. Biotinylated ACE2 (biotin-ACE2) and ExtrAvidin®-peroxidase are used to detect the ACE2:RBD interaction. *o*-Phenylenediamine dihydrochloride (OPD), a peroxidase substrate with absorbance at 450 nm was used for binding visualization. RBD inhibitors that interfere with the ACE2:RBD interaction will lead to a decrease in colorimetric signal.

Table 1 Experimentally measured IC_{50} values of quercetin (**1**) and the *O*-modified quercetin derivatives that exhibited a dose-dependent inhibition against the SARS-CoV-2 S_1:ACE2 interaction

Compound	IC_{50}[a] (μM)
Erythrosine B (EB)	6.16
Quercetin (**1**)	n.d.[b]
2e	7.52
3a	5.00
3b	25.70
3c	2.22
4b	3.28

[a] Average IC_{50} in 3 independent trials (n = 3). [b] Not determined (n.d.), did not exhibit a dose-dependent inhibition at the working concentration range (0.8–100 μM).

The % inhibition of the *O*-modified quercetin derivatives was calculated and presented in Fig. 1. Compounds **2e**, **3a–c**, and **4b** exhibited a dose-dependent inhibition against the SARS-CoV-2 S:ACE2 interaction. Quercetin (**1**) did not exhibit a dose-dependent inhibition and did not reach 50% inhibition even at the highest concentration (100 μM). Compounds **3d**, **3e**, and **5c** showed low inhibition, with <50% inhibition observed even at the highest concentration. Compounds **2a–d**, **4a**, **4c**, and **5a–b** did not display a dose-dependent inhibition within the working concentration range (0.8–100 μM) but showed >50% inhibition even at the lowest concentration.

Analysis of the calculated % inhibition of the derivatives against the SARS-CoV-2 S_1:ACE2 interaction suggests that capping the hydroxyl groups of quercetin with hydrophobic moieties generally results in more potent inhibitors. However, increasing the bulkiness of the R group diminishes the % inhibition of the compounds, as evident in derivatives **3d–e** and **5c**. These findings are consistent with previous studies, which indicate that the inhibition efficacy is influenced by the hydrophobicity of the molecule. Hydrophobic R groups affect the ability of the molecule to assume the bioactive conformation by establishing optimal interactions with the specific amino acid residues in the SARS-CoV-2 S:ACE2 interface that leads to the stabilization of the complex.[24,25,34]

Table 1 presents the IC_{50} values of compounds that exhibited dose-dependent inhibition with erythrosine B (EB) as the positive control. EB is a promiscuous protein–protein interaction (PPI) inhibitor reported to inhibit the SARS-CoV-2 S:ACE2 interaction in low micromolar concentration.[35] The IC_{50} values of compounds that are not dose-dependent were not determined, as this could provide inconclusive results.

Notably, compounds **3a** (IC_{50} = 5.00 μM), **3c** (IC_{50} = 2.22 μM), and **4b** (IC_{50} = 3.28 μM) displayed lower IC_{50} values than

Table 2 Mean % hepato-, nephro-, and cardiotoxicity of quercetin (**1**) and the derivatives that gave a dose-dependent response against the SARS-CoV-2 S:ACE interaction

Compound	Concentration (IC_{50}, ppm)	Hepatotoxicity (%)		Nephrotoxicity (%)		Cardiotoxicity (%)	
		Mean[a]	SEM[b]	Mean[a]	SEM[b]	Mean[a]	SEM[b]
Quercetin (**1**)	30.22	1.74	1.18	1.56	1.32	12.93	9.83
2e	4.71	0.40	0.40	1.29	0.66	1.21	0.62
3a	2.07	1.47	0.36	5.50	1.81	0.11	0.11
3b	12.09	0.39	0.39	1.71	0.51	1.05	0.97
3c	1.03	0.00	0.00	0.04	0.04	1.83	1.60
4b	1.54	0.21	0.21	0.26	0.16	1.95	1.95

[a] Mean % cytotoxicity of 3 independent trials (n = 3). [b] Reported as the standard error of the mean (SEM), n = 3.

erythrosine B (IC_{50} = 6.16 μM), indicating their potential as SARS-CoV-2 S:ACE2 inhibitors. The results also suggest that increasing the chain length of the R group reduces the inhibitory effect of the derivatives, as observed in compounds **3a** and **3b**. However, compound **3c** exhibited an inhibition 10-fold greater than compound **3b**, despite both compounds having identical chain lengths. This observation may be due to the presence of π-electrons in the allyl group of compound **3c**, enabling allyl π-electron-related interactions with the target proteins.[36] Furthermore, compound **2e** exhibited good inhibition against the SARS-CoV-2 S_1:ACE2 interaction, likely due to the presence of the aromatic ring and fluorine moiety. Aromatic groups could participate in π–π stacking interaction with the aromatic residues of the target proteins.[36] Fluorinated molecules have been commonly used in drug discovery due to their lipophilic nature, increasing the molecular stability of the drug.[37] The good inhibitory activity of compound **4b** may be attributed to the introduction of hydrogen bonding acceptors, which can participate in the protein–ligand interaction.[36]

Toxicity assay. Toxicity of drug candidates in the major organ systems specifically the kidney, liver, and heart is the leading cause of attrition in drug development.[38] ACE2 is mainly expressed in myocardial cells and proximal tubule cells of the kidney, rendering them susceptible to SARS-CoV-2 infection.[8] Thus, in this study, the toxicity of the *O*-modified quercetin derivatives, which exhibited a dose-dependent inhibition against the SARS-CoV-2 S:ACE2

Table 3 Summary of the bioavailability and physicochemical properties, pharmacokinetic, drug-likeness, and medicinal chemistry friendliness of quercetin (**1**) and the synthesized *O*-modified quercetin derivatives[a]

	Bioavailability and physicochemical properties						Pharmacokinetics			Drug-likeness		Medicinal chemistry	
	$\log P_{o/w}$ (MLOGP)	MW	nHBD	nHBA	TPSA	nRB				Lipinski (number of violations)	Abbott bioavailability score		
Compound	≤4.15	150–500 Da	≤5	≤10	≤140 Å^2	≤13	HIA	BBB permeant	P-gp substrate	≤1 violations	>0.10	PAINS	Brenk
1	−0.56	302.24	5	7	131.36	1	High	No	No	0	0.55	1	1
2a	0.86	386.40	2	7	98.36	7	High	No	No	0	0.55	0	0
2b	1.50	428.47	2	7	98.36	10	High	No	No	0	0.55	0	0
2c	1.28	422.43	2	7	98.36	10	High	No	No	0	0.55	0	1
2d	3.19	572.60	2	7	98.36	10	Low	No	No	1	0.55	0	0
2e	4.26	626.57	2	10	98.36	10	Low	No	No	2	0.17	0	0
3a	1.29	414.45	1	7	87.36	9	High	No	No	0	0.55	0	0
3b	2.11	470.55	1	7	87.36	13	Low	No	Yes	0	0.55	0	0
3c	1.83	462.49	1	7	87.36	13	High	No	No	0	0.55	0	1
3d	4.20	662.73	1	7	87.36	13	Low	No	No	2	0.17	0	0
3e	5.60	734.69	1	11	87.36	13	Low	No	No	2	0.17	0	0
4a	0.74	428.35	2	10	149.57	7	Low	No	No	0	0.55	0	1
4b	1.38	470.43	2	10	149.57	10	Low	No	No	0	0.55	0	1
4c	3.36	614.55	2	10	149.57	10	Low	No	No	1	0.55	0	1
5a	1.15	470.38	1	11	155.64	9	Low	No	No	1	0.55	0	1
5b	1.98	526.49	1	11	155.64	13	Low	No	No	2	0.17	0	1
5c	4.64	718.66	1	11	155.64	13	Low	No	No	3	0.17	0	1

[a] SwissADME descriptors and their acceptable ranges and response: Moriguchi octanol/water partition coefficient (MLOGP) ≤ 4.15; molecular weight (MW) = 150–500 Da; number of hydrogen bond donor (nHBD) ≤ 5; number of hydrogen bond acceptor (nHBA) ≤ 10; topological surface area (TPSA) ≤ 140 Å^2; number of rotatable bonds (nRB) ≤ 13; human intestinal absorption (HIA): high/low; blood–brain barrier (BBB) permeant: yes/no; P-glycoprotein (P-gp) substrate: yes/no; Lipinski's "Rule of 5" ≤ 1 violations; Abbott bioavailability score > 0.10; pan-assay interference compounds (PAINS) filter: number of alerts; structural alert (Brenk) filter: number of alerts.

interaction, was determined using a CytoTox 96® NonRadioactive Cytotoxicity Assay against HepG2, HK-2, and H9c2 cell lines. This assay is based on the colorimetric measurement of the amount of lactate dehydrogenase (LDH) secreted by cells upon lysis and its reaction with iodonitrotetrazolium (INT) salt, forming a red formazan product. The absorbance of the red formazan product is proportional to the number of lysed cells. The lowest bioactive concentration of the derivatives was used as the test concentration. The criteria used for the classification of cytotoxicity are as follows, non-cytotoxic (<0% cytotoxicity), mildly cytotoxic (0–1%), moderately cytotoxic (1–10%), and highly cytotoxic (>10%).

Table 2 summarizes the mean % cytotoxicity of the derivatives that exhibited a dose-dependent inhibition against the SARS-CoV-2 S:ACE2 interaction. Based on the results, all tested derivatives (*i.e.*, compounds **2e**, **3a–c**, and **4b**) exhibited less than 10% cytotoxicity across all three cell lines. Compared to quercetin, all derivatives showed lower cytotoxicity in all cell lines, except for compound **3a**, which exhibited higher nephrotoxicity. Moreover, only quercetin gave a mean cardiotoxicity greater than 10%. These results imply that all the tested derivatives have the potential to be further developed as lead compounds due to their promising SARS-CoV-2 S:ACE2 inhibition and low toxicity.

Prediction and evaluation of physicochemical properties, pharmacokinetics, drug-likeness, and medicinal chemistry friendliness of the *O*-modified quercetin derivatives

A key aspect of the successful therapeutic action of any drug is its ability to reach the appropriate site of action with a sufficient bioactive concentration.[18] Compounds with high bioactivity and low toxicity are typically considered favorable candidates. However, assessment of the pharmacokinetic and physicochemical profiles is also important to determine the overall drug-likeness of a compound. SwissADME is a valuable web tool used to evaluate the absorption, distribution, metabolism, excretion, and toxicity (ADMET) of drug candidates.[39] Specifically, it aids in predicting bioavailability, physicochemical and pharmacokinetic properties, drug-likeness, and medicinal chemistry friendliness of drug candidates. Table 3 summarizes the calculated parameters of the synthesized compounds using various SwissADME descriptors.

The physicochemical properties associated with oral bioavailability are evaluated through Lipinski's and Veber's rule, which considers parameters such as $\log P_{o/w}$ (MLOGP), molecular weight (MW), number of hydrogen bond donors (nHBD), number of hydrogen bond acceptors (nHBA), topological polar surface area (TPSA) and the number of rotatable bonds (nRB).[40–42] As shown in Table 3, the majority of the synthesized derivatives are within the acceptable limits of the physicochemical descriptors, with some exhibiting minor deviations. For instance, the molecular weights of compounds **2d–e**, **3d–e**, **4c**, and **5b–c** are greater than the 500 Da limit, whereas **4a–c** and **5a–c** showed slightly higher TPSA. While these deviations may suggest poor oral bioavailability, other criteria must be considered to determine the overall suitability of the compound for drug development, as suggested by Veber *et al.*[43]

Human intestinal absorption (HIA) measures the drug absorption properties. The ability of the drug to traverse the intestinal epithelial barrier directly influences the rate and extent of human absorption thus, impacting its bioavailability.[44] Among the synthesized derivatives, compounds **2a–c**, **3a**, and **3c** are predicted to have high HIA, suggesting effective absorption in the body, while compounds **2d–e**, **3d–e**, **4a–c**, and **5a–c** have low HIA. Interestingly, studies suggest that capping the hydroxyl groups of quercetin with hydrophobic moieties enhanced its binding ability with serum albumin as a transporter, thus potentially altering the absorption mechanism.[27,45] Moreover, none of the compounds are expected to permeate the BBB, and almost all are not P-glycoprotein (P-gp) substrates. P-gp substrates participate in the transport of molecules within cells of pharmacokinetic-related organs, such as the gastrointestinal tract and the blood–brain barrier (BBB).[46,47]

Lipinki's filter is the most well-known and widely used method to evaluate drug-likeness, but may not be easily and accurately applicable to complex natural products and multiple halogenated compounds.[44,48] The Abbott bioavailability score is a predictive model used to estimate the likelihood of a compound achieving a minimum of 10% oral bioavailability in rats or measurable Caco-2 permeability.[49] This model is utilized to evaluate the oral bioavailability potential of compounds, particularly those with multiple violations of Lipinski's rule. As presented in Table 3, although some compounds (*i.e.*, **2e**, **3d–e**, and **5b–c**) showed more than one violation of Lipinski's rule, the Abbott bioavailability score for all the synthesized derivatives is within the acceptable range.

The pan-assay interference compounds (PAINS)[50] and Brenk filters[51] are complementary pattern recognition methods, which identify potentially problematic fragments that could react *in vivo* and result in toxic metabolites and reactive species. No alerts in the PAINS filter were observed for all the synthesized derivatives, whereas an alert in the Brenk filter was predicted in some of the compounds. The structural motifs such as the isolated alkene in compounds **2c** and **3c** and the presence of phenol esters in compounds **4a–c**, and **5a–c** might be possible reactive moieties of the derivatives. Nonetheless, previous studies show that quercetin ester derivatives can bypass the phase II metabolism during absorption, resulting in metabolically stable derivatives.[27]

Conclusions

In this study, sixteen (16) *O*-modified quercetin derivatives were synthesized and characterized, and their inhibitory potential targeting the SARS-CoV-2 S:ACE2 interaction was

evaluated. Using an ELISA-type SARS-CoV-2 S:ACE2 inhibition assay, five (5) derivatives showed a dose-dependent response, demonstrating promising inhibitory activity (*i.e.*, **2e** (IC_{50} = 7.52 μM), **3a** (IC_{50} = 5.00 μM), **3b** (IC_{50} = 25.70 μM), **3c** (IC_{50} = 2.22 μM), and **4b** (IC_{50} = 3.28 μM)). Generally, the results showed that incorporating hydrophobic groups to the hydroxyl moieties of quercetin yielded more potent inhibitors with >50% inhibition. However, introducing highly bulky groups decreases the inhibitory activity of the compounds, unless they contain structural elements such as aromatic or pi-donating moieties, fluorinated groups, or hydrogen-bonding acceptors, which could provide additional favorable interactions with the target proteins. The derivatives that exhibited a dose-dependent inhibition displayed less than 10% hepato-, nephro-, and cardiotoxicity, and acceptable physicochemical, pharmacokinetic, and drug-like properties, indicating their possible application as therapeutic agents against COVID-19. Future work on this research warrants further investigations on the *in vivo* potential of these derivatives as SARS-CoV-2 inhibitors. In-depth studies using *in silico* methods and protein–ligand binding experiments are also necessary to fully understand the mechanism of inhibition. Considering the current lack of extensive research on SARS-CoV-2 S:ACE2 inhibitors, this study could promote further development of small molecules as inhibitors targeting the SARS-CoV-2 S:ACE2 interaction.

Experimental section

Synthesis of *O*-modified quercetin derivatives

All reagents were purchased and used as received, without any prior purification, unless otherwise specified. The ^{1}H and ^{13}C NMR spectra were obtained using a Varian 500 MHz spectrometer. Each sample was dissolved with an appropriate deuterated solvent (*i.e.*, $CDCl_3$ or DMSO-d_6). The chemical shifts were expressed in parts per million (ppm) and are referenced to the residual chloroform (7.26 ppm for ^{1}H NMR and 77.16 ppm for ^{13}C NMR) or DMSO (2.50 ppm for ^{1}H NMR and 39.52 ppm for ^{13}C NMR) peaks. Data are presented as follows: chemical shift (δ), multiplicity (s = singlet, d = doublet, dd = doublet of doublet, t = triplet, q = quartet, and m = multiplet), coupling constants (J) in Hz, and proton integration. The infrared (IR) spectrum was acquired using a Shimadzu IR Prestige 21 Fourier-transform infrared spectrometer with an attenuated total reflectance (ATR) accessory and was scanned from 400–4000 cm^{-1}. High-resolution mass spectra were obtained using a Waters Acquity UPLC H-Class Xevo G2XS Quadrupole Time-of-Flight high-resolution mass spectrometer. The melting point range was determined using a Cole Parmer Electrochemical IA9200. Data were reported as uncorrected.

General procedure for the synthesis of *O*-trialkyl derivatives[30]

The reaction vessel was prepared by using a 25 mL oven-dried round bottom flask equipped with a magnetic stir bar and a rubber septum for the nitrogen inlet. To a solution of **1** (100 mg, 0.33 mmol, 1.0 equiv.) in 1.5 mL anhydrous DMF was added anhydrous K_2CO_3 (137 mg, 0.99 mmol, 3.0 equiv.), followed by the dropwise addition of appropriate alkyl halide (1.65 mmol, 5.0 equiv.). The reaction mixture was stirred for 24 hours and the reaction progress was monitored through thin-layer chromatography (TLC). Upon completion, the reaction mixture was partitioned between brine and chloroform (3 × 20 mL). The organic layer was collected, dried over $MgSO_4$, filtered, and concentrated by rotary evaporation. The crude material was purified by gravity column chromatography on silica gel (EtOAc/*n*-hexane = 0 : 100 → 20 : 80), to yield compounds **2a–e**.

3,7-Diethoxy-2-(4-ethoxy-3-hydroxyphenyl)-5-hydroxy-4*H*-chromen-4-one (2a). Yellow-green solid, 61% yield. ^{1}H-NMR (500 MHz, $CDCl_3$) δ (ppm) 12.66 (s, 1H), 7.72 (d, J = 2.2 Hz, 1H), 7.70 (s, 1H), 6.93 (d, J = 8.1 Hz, 1H), 6.41 (d, J = 2.2 Hz, 1H), 6.32 (d, J = 2.2 Hz, 1H), 5.86 (s, 1H), 4.20 (q, J = 7.0 Hz, 2H), 4.08 (q, J = 7.0 Hz, 4H), 1.50 (t, J = 7.0 Hz, 3H), 1.45 (t, J = 7.0 Hz, 3H), 1.35 (t, J = 7.0 Hz, 3H). ^{13}C-NMR (126 MHz, $CDCl_3$) δ (ppm) 179.1, 164.9, 162.0, 156.8, 156.0, 148.1, 145.5, 138.1, 123.7, 121.7, 114.5, 111.0, 106.0, 98.3, 92.5, 68.7, 64.7, 64.3, 15.7, 14.9, 14.7. IR (ATR-FTIR) ν (cm^{-1}) 3406 (O–H stretch), 2980, 2938, 2886 (sp^3 C–H stretch), 1663 (C═O stretch), 1589 (aromatic C–C stretch), 1211 (C–O stretch). HRMS-ESI$^+$ (m/z) calculated for $[M + H]^+$ $C_{21}H_{23}O_7$: 387.1444, found 387.1447. Melting point: 133–134 °C.

5-Hydroxy-2-(3-hydroxy-4-propoxyphenyl)-3,7-dipropoxy-4*H*-chrom-en-4-one (2b). Yellow-green solid, 55% yield. ^{1}H-NMR (500 MHz, $CDCl_3$) δ (ppm) 12.67 (s, 1H), 7.71 (d, J = 2.2 Hz, 1H), 7.69 (s, 1H), 6.93 (d, J = 8.3 Hz, 1H), 6.42 (d, J = 2.2 Hz, 1H), 6.33 (d, J = 2.2 Hz, 1H), 5.74 (s, 1H), 4.10 (t, J = 6.6 Hz, 2H), 3.98 (t, J = 6.6 Hz, 2H), 3.96 (t, J = 6.9 Hz, 2H), 1.94–1.87 (m, 2H), 1.87–1.80 (m, 2H), 1.80–1.71 (m, 2H), 1.08 (t, J = 7.4 Hz, 3H), 1.05 (t, J = 7.4 Hz, 3H), 0.96 (t, J = 7.4 Hz, 3H). ^{13}C-NMR (126 MHz, $CDCl_3$) δ (ppm) 179.1, 165.1, 162.0, 156.9, 155.9, 148.2, 145.6, 138.4, 123.7, 121.8, 114.6, 111.1, 106.1, 98.4, 92.6, 74.6, 70.6, 70.2, 23.5, 22.6, 22.5, 10.6 (2C), 10.5. IR (ATR-FTIR) ν (cm^{-1}) 3304 (O–H stretch), 2967, 2940, 2878 (sp^3 C–H stretch), 1657 (C═O stretch), 1574 (aromatic C–C stretch), 1277 (C–O stretch). HRMS-ESI$^+$ (m/z) calculated for $[M + Na]^+$ $C_{24}H_{28}O_7Na$: 451.1733, found 451.1729. Melting point: 140–141 °C.

3,7-Bis(allyloxy)-2-(4-(allyloxy)-3-hydroxyphenyl)-5-hydroxy-4*H*-chromen-4-one (2c). Yellow-green solid, 56% yield. ^{1}H-NMR (500 MHz, $CDCl_3$) δ (ppm) 12.63 (s, 1H), 7.72–7.67 (m, 2H), 6.93 (d, J = 9.2 Hz, 1H), 6.43 (d, J = 2.2 Hz, 1H), 6.34 (d, J = 2.3 Hz, 1H), 6.16–5.91 (m, 3H), 5.85 (s, 1H), 5.48–5.14 (m, 6H), 4.68 (d, J = 5.5 Hz, 2H), 4.60–4.58 (m, 2H), 4.58–4.56 (m, 2H). ^{13}C-NMR (126 MHz, $CDCl_3$) δ (ppm) δ 178.9, 164.4, 162.0, 156.8, 156.1, 147.8, 145.7, 137.7, 133.5, 132.3, 132.2, 123.9, 121.8, 119.1, 118.8, 118.5, 114.9, 111.6, 106.1, 98.6, 92.9, 73.4, 69.9, 69.3. IR (ATR-FTIR) ν (cm^{-1}) 3181 (O–H stretch), 3082 (sp^2 C–H stretch), 2932, 2872 (sp^3 C–H stretch), 1657 (C═O stretch), 1584 (aromatic C–C stretch), 1259 (C–O stretch). HRMS-ESI$^+$ (m/z) calculated for

$[M + Na]^+$ $C_{24}H_{22}O_7Na$: 445.1263, found 445.1255. Melting point: 70–74 °C.

3,7-Bis(benzyloxy)-2-(4-(benzyloxy)-3-hydroxyphenyl)-5-hydroxy-4*H*-chromen-4-one (2d). Yellow-green solid, 56% yield. ^{1}H-NMR (500 MHz, $CDCl_3$) δ (ppm) 12.72 (s, 1H), 7.64 (s, 1H), 7.62 (d, J = 2.2 Hz, 1H), 7.48–7.34 (m, 12H), 7.30–7.27 (m, 3H), 6.95 (d, J = 9.5 Hz, 1H), 6.49 (d, J = 2.2 Hz, 1H), 6.44 (d, J = 2.2 Hz, 1H), 5.81 (s, 1H), 5.19 (s, 2H), 5.12 (s, 2H), 5.07 (s, 2H). ^{13}C-NMR (126 MHz, $CDCl_3$) δ (ppm) 178.9, 164.5, 162.1, 156.8, 156.4, 148.0, 145.7, 137.7, 136.5, 135.9, 135.8, 129.0 (2C), 128.9 (4C), 128.8, 128.5, 128.4 (2C), 128.3, 128.0 (2C), 127.6 (2C), 124.0, 122.0, 115.0, 111.6, 106.3, 98.8, 93.1, 74.3, 71.2, 70.5. IR (ATR-FTIR) ν (cm^{-1}) 3285 (O–H stretch), 3028 (sp^2 C–H stretch), 2936, 2878 (sp^3 C–H stretch), 1655 (C═O stretch), 1599, 1576 (aromatic C–C stretch), 1279 (C–O stretch). HRMS-ESI$^+$ (m/z) calculated for $[M + Na]^+$ $C_{36}H_{28}O_7Na$: 595.1733, found 595.1741. Melting point: 148–153 °C.

3,7-Bis((4-fluorobenzyl)oxy)-2-(4-((4-fluorobenzyl)oxy)-3-hydroxy-phenyl)-5-hydroxy-4*H*-chromen-4-one (2e). Yellow-green solid, 78% yield. ^{1}H-NMR (500 MHz, $CDCl_3$) δ (ppm) 12.66 (s, 1H), 7.62 (s, 1H), 7.57 (d, J = 8.7 Hz, 1H), 7.46–7.37 (m, 4H), 7.33 (dd, J = 8.7, 5.5 Hz, 2H), 7.11 (t, J = 8.6 Hz, 2H), 7.09 (t, J = 8.7 Hz, 2H), 6.94 (t, J = 8.7 Hz, 3H), 6.46 (s, 1H), 6.40 (s, 1H), 5.86 (s, 1H), 5.14 (s, 2H), 5.06 (s, 2H), 5.01 (s, 2H). ^{13}C-NMR (126 MHz, $CDCl_3$) δ (ppm) 178.9, 164.4, 162.9 (d, $J_{C,F}$ = 248.3 Hz, 1C), 162.7 (d, $J_{C,F}$ = 247.3 Hz, 2C), 162.1, 156.8, 156.5, 145.7, 137.9, 137.5, 132.3 (d, $J_{C,F}$ = 3.4 Hz, 1C), 131.5 (d, $J_{C,F}$ = 3.4 Hz, 1C), 131.4 (d, $J_{C,F}$ = 3.3 Hz, 1C), 130.7 (d, $J_{C,F}$ = 8.6 Hz, 2C), 129.9 (d, $J_{C,F}$ = 8.1 Hz, 2C), 129.4 (d, $J_{C,F}$ = 8.1 Hz, 2C), 124.1, 121.9, 115.9 (d, $J_{C,F}$ = 22.0 Hz, 2C), 115.7 (d, $J_{C,F}$ = 22.0 Hz, 2C), 115.1 (d, $J_{C,F}$ = 21.5 Hz, 2C), 115.2, 111.6, 106.3, 98.7, 93.1, 73.6, 70.6, 69.9. IR (ATR-FTIR) ν (cm^{-1}) 3076 (sp^2 C–H stretch), 2922, 2870 (sp^3 C–H stretch), 1655 (C═O stretch), 1599 (aromatic C–C stretch), 1283 (C–O stretch), 1223 (C–F stretch). HRMS-ESI$^+$ (m/z) calculated for $[M + H]^+$ $C_{36}H_{26}O_7F_3$: 627.1631, found 627.1640. Melting point: 144–145 °C.

General procedure for the synthesis of *O*-tetraalkyl derivatives[30]

The reaction vessel was prepared by using a 25 mL oven-dried round bottom flask equipped with a magnetic stir bar and a rubber septum for the nitrogen inlet. To a solution of **1** (100 mg, 0.33 mmol, 1.0 equiv.) in 1.5 mL anhydrous DMF was added anhydrous K_2CO_3 (229 mg, 1.65 mmol, 5.0 equiv.), followed by the dropwise addition of appropriate alkyl halide (1.65 mmol, 5.0 equiv.). The reaction mixture was stirred for 24 hours and the reaction progress was monitored through thin-layer chromatography (TLC). Upon completion, the reaction mixture was partitioned between brine and chloroform (3 × 20 mL). The organic layer was collected, dried over $MgSO_4$, filtered, and concentrated by rotary evaporation. The crude material was purified by gravity column chromatography on silica gel (EtOAc/*n*-hexane = 0 : 100 → 20 : 80), to yield compounds **3a–e**.

2-(3,4-Diethoxyphenyl)-3,7-diethoxy-5-hydroxy-4*H*-chromen-4-one (3a). Yellow-green solid, 50% yield. ^{1}H-NMR (500 MHz, $CDCl_3$) δ (ppm) 12.67 (s, 1H), 7.73 (d, J = 2.2 Hz, 1H), 7.68 (dd, J = 8.6, 2.2 Hz, 1H), 6.96 (d, J = 8.7 Hz, 1H), 6.40 (d, J = 2.2 Hz, 1H), 6.31 (d, J = 2.2 Hz, 1H), 4.17 (q, J = 7.0 Hz, 2H), 4.16 (q, J = 7.0 Hz, 2H), 4.08 (q, J = 7.0 Hz, 2H), 4.05 (q, J = 7.0 Hz, 2H), 1.50 (t, J = 7.0 Hz, 3H), 1.49 (t, J = 7.0 Hz, 3H), 1.43 (t, J = 7.0 Hz, 3H), 1.33 (t, J = 7.1 Hz, 3H). ^{13}C-NMR (126 MHz, $CDCl_3$) δ (ppm) 179.0, 164.9, 162.1, 156.8, 156.3, 151.2, 148.2, 138.0, 123.1, 122.2, 113.7, 112.3, 106.0, 98.2, 92.7, 68.7, 64.9, 64.6, 64.3, 15.7, 14.9, 14.8, 14.7. IR (ATR-FTIR) ν (cm^{-1}) 2980, 2938, 2874 (sp^3 C–H stretch), 1659 (C═O stretch), 1589 (aromatic C–C stretch), 1277 (C–O stretch). HRMS-ESI$^+$ (m/z) calculated for $[M + H]^+$ $C_{23}H_{27}O_7$: 415.1757, found 415.1750. Melting point: 124–125 °C.

2-(3,4-Dipropoxyphenyl)-5-hydroxy-3,7-dipropoxy-4*H*-chromen-4-one (3b). Yellow-green solid, 44% yield. ^{1}H-NMR (500 MHz, $CDCl_3$) δ (ppm) 12.69 (s, 1H), 7.71 (d, J = 2.2 Hz, 1H), 7.68 (dd, J = 8.5, 2.2 Hz, 1H), 6.96 (d, J = 8.6 Hz, 1H), 6.42 (d, J = 2.2 Hz, 1H), 6.33 (d, J = 2.2 Hz, 1H), 4.04 (t, J = 6.7 Hz, 2H), 4.03 (t, J = 6.6 Hz, 2H), 3.97 (t, J = 6.5 Hz, 2H), 3.94 (t, J = 6.9 Hz, 2H), 1.93–1.86 (m, 4H), 1.85–1.79 (m, 2H), 1.78–1.70 (m, 2H), 1.10–1.02 (m, 9H), 0.95 (t, J = 7.5 Hz, 3H). ^{13}C-NMR (126 MHz, $CDCl_3$) δ (ppm) 179.0, 165.0, 162.0, 156.8, 156.3, 151.6, 148.5, 138.2, 123.0, 122.4, 114.2, 112.5, 106.0, 98.2, 92.7, 74.7, 71.0, 70.5, 70.2, 23.5, 22.7, 22.6, 22.5, 10.6 (3C), 10.5. IR (ATR-FTIR) ν (cm^{-1}) 2876 (sp^3 C–H stretch), 1661 (C═O stretch), 1587 (aromatic C–C stretch), 1275 (C–O stretch). HRMS-ESI$^+$ (m/z) calculated for $[M + Na]^+$ $C_{27}H_{34}O_7Na$: 493.2202, found 493.2195. Melting point: 91–93 °C.

3,7-Bis(allyloxy)-2-(3,4-bis(allyloxy)phenyl)-5-hydroxy-4*H*-chromen-4-one (3c). Yellow-green solid, 42% yield. ^{1}H-NMR (500 MHz, $CDCl_3$) δ (ppm) 12.64 (s, 1H), 7.75 (d, J = 2.1 Hz, 1H), 7.68 (dd, J = 8.4, 2.2 Hz, 1H), 6.97 (d, J = 8.7 Hz, 1H), 6.43 (d, J = 2.2 Hz, 1H), 6.35 (d, J = 2.2 Hz, 1H), 6.15–5.90 (m, 4H), 5.49–5.40 (m, 3H), 5.36–5.28 (m, 4H), 5.20–5.16 (m, 1H), 4.69 (dt, J = 5.3, 1.6 Hz, 2H), 4.65 (dt, J = 5.3, 1.5 Hz, 2H), 4.59 (dt, J = 5.3, 1.5 Hz, 2H), 4.56 (dt, J = 6.0, 1.3 Hz, 2H). ^{13}C-NMR (126 MHz, $CDCl_3$) δ (ppm) 178.9, 164.5, 162.1, 156.8, 156.2, 151.0, 148.1, 137.6, 133.6, 133.2, 132.9, 132.3, 123.3, 122.5, 118.7, 118.5, 118.2, 118.1, 114.4, 113.0, 106.1, 98.5, 93.0, 73.5, 70.2, 69.8, 69.3. IR (ATR-FTIR) ν (cm^{-1}) 3084, 3015 (sp^2 C–H stretch), 2924, 2870 (sp^3 C–H stretch), 1663 (C═O stretch), 1585 (aromatic C–C stretch), 1321 (C–O stretch). HRMS-ESI$^+$ (m/z) calculated for $[M + Na]^+$ $C_{27}H_{26}O_7Na$: 485.1576, found 485.1588. Melting point: 68–71 °C.

3,7-Bis(benzyloxy)-2-(3,4-bis(benzyloxy)phenyl)-5-hydroxy-4*H*-chromen-4-one (3d). Yellow-green solid, 87% yield. ^{1}H-NMR (500 MHz, $CDCl_3$) δ (ppm) 12.72 (s, 1H), 7.73 (d, J = 2.1 Hz, 1H), 7.57 (dd, J = 8.6, 2.1 Hz, 1H), 7.52–7.22 (m, 20H), 6.97 (d, J = 8.6 Hz, 1H), 6.47 (d, J = 2.2 Hz, 1H), 6.45 (d, J = 2.3 Hz, 1H), 5.26 (s, 2H), 5.13 (s, 2H), 5.05 (s, 2H), 5.00 (s, 2H). ^{13}C-NMR (126 MHz, $CDCl_3$) δ (ppm) 178.9, 164.6, 162.2,

156.8, 156.4, 151.2, 148.3, 137.6, 137.0, 136.8, 136.6, 135.9, 128.9 (4C), 128.7 (2C), 128.6 (2C), 128.5, 128.4 (3C), 128.1, 128.0, 127.6 (2C), 127.5 (2C), 127.3 (2C), 123.5, 122.7, 115.4, 113.8, 106.3, 98.7, 93.2, 74.5, 71.2, 71.0, 70.6. IR (ATR-FTIR) ν (cm^{-1}) 3300 (O–H stretch), 3062, 3030 (sp^2 C–H stretch), 2924, 2878 (sp^3 C–H stretch), 1657 (C═O stretch), 1587 (aromatic C–C stretch), 1277 (C–O stretch). HRMS-ESI$^+$ (m/z) calculated for $[M + H]^+$ $C_{43}H_{35}O_7$: 663.2383, found 663.2390. Melting point: 141–144 °C.

2-(3,4-Bis((4-fluorobenzyl)oxy)phenyl)-3,7-bis((4-fluorobenzyl)oxy)-5-hydroxy-4*H*-chromen-4-one (3e). Yellow-green solid, 61% yield. ^{1}H-NMR (500 MHz, $CDCl_3$) δ (ppm) 12.65 (s, 1H), 7.66 (s, 1H), 7.56 (d, J = 8.6 Hz, 1H), 7.47–7.34 (m, 6H), 7.28–7.22 (m, 2H), 7.16–7.02 (m, 6H), 7.00–6.89 (m, 3H), 6.44 (d, J = 11.5 Hz, 2H), 5.19 (s, 2H), 5.09 (s, 2H), 5.02 (s, 2H), 4.96 (s, 2H). ^{13}C-NMR (126 MHz, $CDCl_3$) δ (ppm) 178.8, 164.5, 162.2, 162.8 (d, $J_{C,F}$ = 247.8 Hz, 1C), 162.7 (d, $J_{C,F}$ = 247.8 Hz, 1C), 162.6 (d, $J_{C,F}$ = 247.3 Hz, 1C), 162.5 (d, $J_{C,F}$ = 246.8 Hz, 1C), 156.8, 156.4, 151.1, 148.2, 137.4, 132.6 (d, $J_{C,F}$ = 3.4 Hz, 1C), 132.4 (d, $J_{C,F}$ = 3.4 Hz, 1C), 132.2 (d, $J_{C,F}$ = 3.3 Hz, 1C), 131.6 (d, $J_{C,F}$ = 2.9 Hz, 1C), 130.8 (d, $J_{C,F}$ = 8.6 Hz, 2C), 129.5 (d, $J_{C,F}$ = 8.1 Hz, 2C), 129.3 (d, $J_{C,F}$ = 8.1 Hz, 2C), 129.2 (d, $J_{C,F}$ = 8.6 Hz, 2C), 123.7, 123.0, 115.8 (d, $J_{C,F}$ = 21.5 Hz, 2C), 115.7 (d, $J_{C,F}$ = 22.0 Hz, 2C), 115.6 (d, $J_{C,F}$ = 21.5 Hz, 2C), 115.5, 115.3 (d, $J_{C,F}$ = 21.5 Hz, 2C), 113.8, 106.2, 98.7, 93.2, 73.7, 70.8, 70.4, 69.9. IR (ATR-FTIR) ν (cm^{-1}) 3088 (sp^2 C–H stretch), 2922, 2857 (sp^3 C–H stretch), 1659 (C═O stretch), 1597 (aromatic C–C stretch), 1279 (C–O stretch), 1225 (C–F stretch). HRMS-ESI$^+$ (m/z) calculated for $[M + H]^+$ $C_{43}H_{31}O_7F_4$: 735.2006, found 735.1970. Melting point: 169–171 °C.

General procedure for the synthesis of *O*-acyl derivatives[31]

To a solution of **1** (100 mg, 0.33 mmol, 1.0 equiv.) in 2.5 mL DCM was added pyridine (0.535 mL, 6.62 mmol, 20.0 equiv.), followed by the dropwise addition of the corresponding acyl chloride (1.16 mmol, 3.5 equiv.). The reaction mixture was stirred for 2 hours, and the reaction progress was monitored through TLC. Upon completion, the reaction mixture was partitioned between brine solution and chloroform (3 × 20 mL). The organic layer was collected, dried over $MgSO_4$, filtered, and concentrated by rotary evaporation. The solids were then washed with cyclohexane to remove the excess pyridine. *O*-Tri (compounds **4a–c**) and -tetraacyl (compounds **5a–c**) derivatives were purified and isolated by gravity column chromatography on silica gel ($MeOH/CHCl_3$ = 0 : 100 → 3 : 97).

2-(4-Acetoxy-3-hydroxyphenyl)-5-hydroxy-4-oxo-4*H*-chromene-3,7-diyl diacetate (4a). Yellow-green solid, 15% yield. ^{1}H-NMR (500 MHz, DMSO-d_6) δ (ppm) 12.04 (s, 1H), 7.84 (s, 1H), 7.82 (s, 1H), 7.52 (d, J = 8.5 Hz, 1H), 6.53 (s, 1H), 6.29 (s, 1H), 2.33 (s, 9H). ^{13}C-NMR (126 MHz, DMSO-d_6) δ (ppm) 175.0, 168.3, 168.2, 168.1, 165.2, 161.1, 156.9, 154.1, 144.5, 142.3, 131.1, 127.3, 126.8, 124.6, 123.8, 103.8, 99.5, 94.5, 20.5 (2C), 20.2. IR (ATR-FTIR) ν (cm^{-1}) 3337 (O–H stretch), 3078 (sp^2 C–H stretch), 2936 (sp^3 C–H stretch), 1773, 1736, 1655 (C═O stretch), 1605 (aromatic C–C stretch), 1172 (C–O stretch). HRMS-ESI$^+$ (m/z) calculated for $[M + Na]^+$ $C_{21}H_{16}O_{10}Na$: 451.0641, found 451.0643. Melting point: 201–204 °C.

5-Hydroxy-2-(3-hydroxy-4-(propionyloxy)phenyl)-4-oxo-4*H*-chrom-ene-3,7-diyl dipropionate (4b). Yellow-green solid, 15% yield. ^{1}H-NMR (500 MHz, DMSO-d_6) δ (ppm) 12.03 (s, 1H), 7.82 (d, J = 8.7 Hz, 1H), 7.80 (s, 1H), 7.51 (d, J = 8.4 Hz, 1H), 6.53 (s, 1H), 6.29 (s, 1H), 2.68–2.60 (m, 6H), 1.17–1.10 (m, 9H). ^{13}C-NMR (126 MHz, DMSO-d_6) δ (ppm) 175.0, 171.6, 171.4 (2C), 165.1, 161.1, 156.9, 154.1, 144.5, 142.2, 131.1, 127.3, 126.7, 124.6, 123.7, 103.8, 99.4, 94.5, 26.8, 26.7, 26.6, 8.9 (2C), 8.8. IR (ATR-FTIR) ν (cm^{-1}) 3404 (O–H stretch), 2982, 2945, 2887 (sp^3 C–H stretch), 1767, 1728, 1657 (C═O stretch), 1616 (aromatic C–C stretch), 1172 (C–O stretch). HRMS-ESI$^+$ (m/z) calculated for $[M + H]^+$ $C_{24}H_{23}O_{10}$: 471.1291, found 471.1312. Melting point: 183–187 °C.

2-(4-(Benzoyloxy)-3-hydroxyphenyl)-5-hydroxy-4-oxo-4*H*-chromene-3,7-diyl dibenzoate (4c). Yellow-green solid, 10% yield. ^{1}H-NMR (500 MHz, DMSO-d_6) δ (ppm) 11.99 (s, 1H), 8.17 (d, J = 8.1 Hz, 2H), 8.00 (d, J = 8.6 Hz, 1H), 7.97–7.88 (m, 4H), 7.79–7.70 (m, 2H), 7.68–7.55 (m, 5H), 7.45 (t, J = 6.6 Hz, 4H), 6.60 (s, 1H), 6.32 (s, 1H). ^{13}C-NMR (126 MHz, DMSO-d_6) δ (ppm) 174.9, 167.4, 165.2, 163.5, 163.4 (2C), 161.2, 157.0, 144.7, 142.5, 134.8, 134.5, 132.9 (2C), 131.5, 130.8, 130.2 (2C), 130.1, 129.8 (2C), 129.7, 129.3 (2C), 129.2, 129.1 (2C), 128.6 (2C), 127.7 (2C), 124.7, 124.0, 103.9, 99.6, 94.7. IR (ATR-FTIR) ν (cm^{-1}) 3439 (O–H stretch), 3066 (sp^2 C–H stretch), 1747, 1734, 1726, 1660 (C═O stretch), 1612, 1593 (aromatic C–C stretch), 1177 (C–O stretch). HRMS-ESI$^+$ (m/z) calculated for $[M + H]^+$ $C_{36}H_{23}O_{10}$: 615.1291, found 615.1284. Melting point: 212–215 °C.

4-(3,7-Diacetoxy-5-hydroxy-4-oxo-4*H*-chromen-2-yl)-1,2-phenylene diacetate (5a). Yellow-green solid, 14% yield. ^{1}H-NMR (500 MHz, $CDCl_3$) δ (ppm) 12.09 (s, 1H), 7.76–7.72 (m, 2H), 7.36 (d, J = 8.1 Hz, 1H), 6.85 (s, 1H), 6.60 (s, 1H), 2.36 (s, 3H), 2.33 (s, 9H). ^{13}C-NMR (126 MHz, $CDCl_3$) δ (ppm) δ 176.4, 168.3, 168.0 (2C), 167.9, 161.8, 156.5, 156.0, 155.7, 144.7, 142.3, 132.3, 127.6, 126.7, 124.1 (2C), 108.9, 105.6, 101.3, 21.3, 20.8 (2C), 20.5. IR (ATR-FTIR) ν (cm^{-1}) 3084 (sp^2 C–H stretch), 2940 (sp^3 C–H stretch) 1771, 1759, 1649 (C═O stretch), 1610 (aromatic C–C stretch), 1200, 1180 (C–O stretch). HRMS-ESI$^+$ (m/z) calculated for $[M + Na]^+$ $C_{23}H_{18}O_{11}Na$: 493.0747, found 493.0787. Melting point: 172–175 °C.

2-(3,4-Bis(propionyloxy)phenyl)-5-hydroxy-4-oxo-4*H*-chromene-3,7-diyl dipropionate (5b). Yellow-green solid, 24% yield. ^{1}H-NMR (500 MHz, $CDCl_3$) δ (ppm) 12.10 (s, 1H), 7.75–7.70 (m, 2H), 7.35 (d, J = 8.4 Hz, 1H), 6.85 (s, 1H), 6.58 (s, 1H), 2.68 (q, J = 7.6 Hz, 2H), 2.63–2.57 (m, 6H), 1.31–1.18 (m, 12H). ^{13}C-NMR (126 MHz, $CDCl_3$) δ (ppm) 176.4, 171.9, 171.5 (2C), 171.4, 161.8, 156.6, 156.0, 155.6, 144.8, 142.4, 132.3, 127.6, 126.6, 124.1 (2C), 108.8, 105.6, 101.3, 27.9, 27.6, 27.6, 27.3, 9.2, 9.2, 9.0, 8.9. IR (ATR-FTIR) ν (cm^{-1}) 3084 (sp^2 C–H stretch), 2984, 2945 (sp^3 C–H stretch) 1765, 1651 (C═O stretch), 1611 (aromatic C–C stretch), 1196 (C–O stretch).

HRMS-ESI$^+$ (m/z) calculated for [M + Na]$^+$ $C_{27}H_{26}O_{11}Na$: 549.1373, found 549.1379. Melting point: 131–134 °C.

4-(3,7-Bis(benzoyloxy)-5-hydroxy-4-oxo-4*H*-chromen-2-yl)-1,2-phenylene dibenzoate (5c). Yellow-green solid, 39% yield. ^{1}H-NMR (500 MHz, $CDCl_3$) δ (ppm) 12.17 (s, 1H), 8.25 (dd, J = 8.4, 1.3 Hz, 2H), 8.21 (dd, J = 8.4, 1.3 Hz, 2H), 8.05–8.01 (m, 4H), 7.95 (dd, J = 8.6, 2.1 Hz, 1H), 7.69–7.63 (m, 2H), 7.60–7.47 (m, 8H), 7.41–7.34 (m, 4H), 7.07 (d, J = 2.0 Hz, 1H), 6.78 (d, J = 2.1 Hz, 1H). ^{13}C-NMR (126 MHz, $CDCl_3$) δ (ppm) 176.4, 164.1, 163.9, 163.8, 163.7, 161.9, 156.9, 156.1, 155.6, 145.4, 143.0, 134.3, 134.2, 134.1, 134.0, 132.8, 130.8 (2C), 130.4 (2C), 130.3 (4C), 128.9 (2C), 128.8 (3C), 128.7 (4C), 128.4, 128.4, 128.1, 127.8, 126.9, 124.3, 124.0, 109.0, 105.9, 101.5. IR (ATR-FTIR) ν (cm^{-1}) 3125, 3073 (sp^2 C–H stretch), 1742, 1655 (C═O stretch), 1601 (aromatic C–C stretch), 1234, 1193, 1173 (C–O stretch). HRMS-ESI$^+$ (m/z) calculated for [M + Na]$^+$ $C_{43}H_{26}O_{11}Na$: 741.1373, found 741.1345. Melting point: 193–195 °C.

Prediction of the physicochemical and pharmacokinetic properties of the *O*-modified quercetin derivatives using SwissADME

The SwissADME web tool,[39] which is accessible at **http://www.swissadme.ch**, was used to determine the physicochemical and pharmacokinetic properties of the designed *O*-modified quercetin derivatives. The molecules of interest were converted to SMILES format imported from ChemAxon's Marvin JS in the input zone. The output for the SwissADME tool contains the chemical structure and bioavailability radar, physicochemical descriptors, lipophilicity, water-solubility, pharmacokinetics, drug-likeness, and medicinal chemistry properties of the compounds.

SARS-CoV-2 S (RBD):ACE2 inhibition assay

Evaluation of the inhibitory capability of the synthesized derivatives against the SARS-CoV-2 S:ACE2 interaction was assessed using a SARS-CoV-2 inhibitor screening kit (Sigma Aldrich CS2000) based on S_1:ACE2 binding colorimetric assay according to the manufacturer's protocol. Briefly, each well of a 96-well plate was coated with 100 μL of 2 μg mL^{-1} SARS-CoV-2 S_1 receptor binding domain (RBD) coating solution and incubated for 60 minutes at 37 °C. The contents of each well were aspirated, discarded, and washed with 200 μL phosphate-buffered saline with 0.05% TWEEN® 20, pH 7.2–7.4 (PBS-T). The contents were aspirated and discarded, and the process was repeated three times. The wells were then blocked with 150 μL of 1% bovine serum albumin (BSA) in 0.01 M phosphate-buffered saline, pH 7.2–7.4 (PBS), and incubated for 30 minutes at 37 °C. The contents of each well were aspirated and discarded and the washing step was repeated. Samples with varying concentrations (100.0, 20.0, 4.0, and 0.8 μM) were then added to the sample wells (50 μL per well). A 0.05% DMSO–PBS solution was then added to the negative control (50 μL per well) and blank wells (100 μL per well) and the plate was incubated for 60 minutes at 37 °C. After the incubation, 50 μL of 0.5 μg mL^{-1} of the biotin-ACE2 solution was added to the sample and negative control wells. The plate was incubated for another 60 minutes at 37 °C. The contents of each well were then aspirated and discarded and the washing step was repeated. 100 μL of ExtrAvidin®-Peroxidase was then added to each well and incubated for 40 minutes at 37 °C. The contents of each well were then aspirated and discarded and the washing step was repeated. 100 μL of the SIGMAFAST™ OPD solution was then added to each well. The plate was incubated and protected from light for 10 minutes at room temperature. The absorbance of the resulting solution was then read at 450 nm using a Thermo Scientific™ Multiskan™ GO Microplate Spectrophotometer. Three trials were performed for each sample.

The % inhibition of the compounds was then calculated. For compounds that exhibited a dose-dependent inhibition against the SARS-CoV-2 S:ACE2 interaction, the half-maximal inhibitory concentration (IC_{50}) was obtained using a GraphPad Prism 9 software by fitting the data points using the nonlinear regression function log(inhibitor) *vs.* response–variable slope (four parameters), where the minimum response was set to 0 and the Hill slope was set to 1.

Toxicity assay

The toxicity of the bioactive compounds was determined by a CytoTox 96® NonRadioactive Cytotoxicity Assay (Promega). Samples were prepared and submitted to the National Institute of Molecular Biology and Biotechnology, Disease Molecular Biology and Epigenetics Laboratory (NIMBB-DMBEL) at the University of the Philippines Diliman. The toxicity of the bioactive compounds was tested at their lowest bioactive concentration against three cell lines: human liver carcinoma (HepG2), human kidney-2 (HK-2), and rat cardiomyoblast (H9c2) cells. HepG2, HK-2, and H9c2 cells were previously obtained from the American Type Culture Collection (ATCC). HepG2 cells were grown in modified Eagle medium (MEM) supplemented with 10% fetal bovine serum (FBS), HK-2 cells were cultured in Dulbecco's modified Eagle medium: nutrient mixture F-12 (DMEM-F12) supplemented with 5% FBS, and H9c2 cells were grown in Dulbecco's modified Eagle medium supplemented with 10% FBS. All media were supplemented with 1% penicillin–streptomycin. All cell lines were incubated at 37 °C, 5% CO_2. Cells were grown to 70–90% confluency for cell maintenance before seeding for assays.

The cells were seeded in a 96-well plate with a 5.0×10^3 cells per mL seeding density. The test compounds were added to the wells to achieve a 100–150 μL volume and incubated at 37 °C for 30 minutes. Independently, a maximum LDH release control was prepared by setting up triplicate wells, and a 10 μL lysis solution was added to each well and incubated at 37 °C for 45 minutes. After incubation, 50 μL aliquots were transferred to a fresh 96-well plate, and 50 μL CytoTox 96® reagent was added to each well. The plate was incubated for another 30 minutes at room temperature. A 50 μL Stop Solution was added to each well, and the absorbance values were measured at 490 nm. The percent cytotoxicity was calculated based on the measured

absorbance of the samples and the control solution. Compounds with a percent toxicity of greater than or equal to 10% were flagged as toxic.

Data availability

The data that supports the findings of this article (*e.g.* ^{1}H and ^{13}C NMR spectra and raw data for the assays) are included in the ESI.†

Author contributions

Synthesis and characterization, methodology, investigation, and formal analysis, R. J. Z. R.; writing – original draft, review, and editing, R. J. Z. R. and M. C. P.; conceptualization, validation, funding acquisition, supervision, and project administration, M. C. P.

Conflicts of interest

The authors declare no conflict of interest.

Acknowledgements

The authors would like to express their utmost gratitude to the Grants-in-Aid (GIA) program of the Department of Science and Technology (DOST) and the DOST-Philippine Council for Health Research and Development (DOST-PCHRD) for funding this research under the program 'Technical Battle Against COVID-19' and project 'Rational Design and Structural Modifications of ACE2 Inhibitors from Terrestrial Plants'. The authors would also like to thank the following facilities: NMR Services Facility, Analytical Services Laboratory, and Mass Spectrometry Facility, Institute of Chemistry, University of the Philippines Diliman, for providing their services for the characterization work; the Bioorganic and Natural Products Laboratory, Institute of Chemistry, University of the Philippines Diliman, for the use of their facilities in conducting the *in vitro* inhibition assays; and the Disease Molecular Biology and Epigenetics Laboratory, National Institute of Molecular Biology and Biotechnology, University of the Philippines Diliman, for conducting the cytotoxicity assay.

References

1 C. Sohrabi, Z. Alsafi, N. O'Neill, M. Khan, A. Kerwan, A. Al-Jabir, C. Iosifidis and R. Agha, *Int. J. Surg.*, 2020, **76**, 71–76.
2 W. Cui, K. Yang and H. Yang, *Front. Mol. Biosci.*, 2020, **7**, 616341.
3 P. Zhou, X.-L. Yang, X.-G. Wang, B. Hu, L. Zhang, W. Zhang, H.-R. Si, Y. Zhu, B. Li, C.-L. Huang, H.-D. Chen, J. Chen, Y. Luo, H. Guo, R.-D. Jiang, M.-Q. Liu, Y. Chen, X.-R. Shen, X. Wang, X.-S. Zheng, K. Zhao, Q.-J. Chen, F. Deng, L.-L. Liu, B. Yan, F.-X. Zhan, Y.-Y. Wang, G.-F. Xiao and Z.-L. Shi, *Nature*, 2020, **579**, 270–273.
4 WHO Coronavirus (COVID-19) Dashboard, **https://covid19.who.int**, (accessed 2024-03-04).
5 F. Li, *Annu. Rev. Virol.*, 2016, **3**, 237–261.
6 S. Perlman and J. Netland, *Nat. Rev. Microbiol.*, 2009, **7**, 439–450.
7 J. Shang, Y. Wan, C. Luo, G. Ye, Q. Geng, A. Auerbach and F. Li, *Proc. Natl. Acad. Sci. U. S. A.*, 2020, **117**, 11727–11734.
8 W. Ni, X. Yang, D. Yang, J. Bao, R. Li, Y. Xiao, C. Hou, H. Wang, J. Liu, D. Yang, Y. Xu, Z. Cao and Z. Gao, *Crit. Care*, 2020, **24**, 422.
9 N. T. Tzvetkov, K. Kirilov, M. Matin and A. G. Atanasov, *Nephrol., Dial., Transplant.*, 2023, **39**, 375–378.
10 H. Hasnat, S. A. Shompa, M. M. Islam, S. Alam, F. T. Richi, N. U. Emon, S. Ashrafi, N. U. Ahmed, M. N. R. Chowdhury, N. Fatema, M. S. Hossain, A. Ghosh and F. Ahmed, *Heliyon*, 2024, **10**, e27533.
11 J. A. P. Francisco and M. C. Paderes, *ACS Omega*, 2023, **8**, 43109–43117.
12 R. D. Hernandez, F. A. F. Genio, J. R. Casanova, M. T. Conato and M. C. Paderes, *ChemistryOpen*, 2024, **13**, e202300087.
13 D. Szabó, A. Crowe, C. Mamotte and P. Strappe, *Front. Cell. Infect. Microbiol.*, 2024, **14**, 1353971.
14 Y. Li, J. Yao, C. Han, J. Yang, M. T. Chaudhry, S. Wang, H. Liu and Y. Yin, *Nutrients*, 2016, **8**, 167.
15 J. S. Mani, J. B. Johnson, J. C. Steel, D. A. Broszczak, P. M. Neilsen, K. B. Walsh and M. Naiker, *Virus Res.*, 2020, **284**, 197989.
16 D.-h. Zhang, K.-l. Wu, X. Zhang, S.-q. Deng and B. Peng, *J. Integr. Med.*, 2020, **18**, 152–158.
17 M. Sopjani, F. Falco, F. Impellitteri, V. Guarrasi, X. Nguyen Thi, M. Dërmaku-Sopjani and C. Faggio, *Phytother. Res.*, 2024, **38**, 1589–1609.
18 G. Williamson and A. Kerimi, *Biochem. Pharmacol.*, 2020, **178**, 114123.
19 M. Muchtaridi, M. Fauzi, N. K. Khairul Ikram, A. Mohd Gazzali and H. A. Wahab, *Molecules*, 2020, **25**, 3980.
20 A. d. S. Antonio, L. S. M. Wiedemann and V. F. Veiga-Junior, *RSC Adv.*, 2020, **10**, 23379–23393.
21 C. Mouffouk, S. Mouffouk, S. Mouffouk, L. Hambaba and H. Haba, *Eur. J. Pharmacol.*, 2021, **891**, 173759.
22 M. Dong, J. M. Galvan Achi, R. Du, L. Rong and Q. Cui, *Cell Insight*, 2024, **3**, 100144.
23 L.-l. Ma, H.-m. Liu, X.-m. Liu, X.-y. Yuan, C. Xu, F. Wang, J.-z. Lin, R.-c. Xu and D.-k. Zhang, *Eur. J. Med. Chem.*, 2021, **226**, 113857.
24 M. Ye, G. Luo, D. Ye, M. She, N. Sun, Y.-J. Lu and J. Zheng, *Phytomedicine*, 2021, **85**, 153401.
25 B. Pan, S. Fang, J. Zhang, Y. Pan, H. Liu, Y. Wang, M. Li and L. Liu, *Comput. Struct. Biotechnol. J.*, 2020, **18**, 3518–3527.
26 A. F. Almeida, G. I. A. Borge, M. Piskula, A. Tudose, L. Tudoreanu, K. Valentová, G. Williamson and C. N. Santos, *Compr. Rev. Food Sci. Food Saf.*, 2018, **17**, 714–731.
27 S. H. Thilakarathna and H. P. Rupasinghe, *Nutrients*, 2013, **5**, 3367–3387.
28 T. Walle, *Mol. Pharmaceutics*, 2007, **4**, 826–832.

29 M. Danihelová, J. Viskupičová and E. Šturdík, *Acta Chim. Slov.*, 2012, **5**, 59–69.
30 S. Al-Jabban, X. Zhang, C. Guanglin, E. Mekuria, L. Harinantenaina and Q.-H. Chen, *Nat. Prod. Commun.*, 2015, **10**, 2113–2118.
31 A. Mattarei, L. Biasutto, F. Rastrelli, S. Garbisa, E. Marotta, M. Zoratti and C. Paradisi, *Molecules*, 2010, **15**, 4722–4736.
32 K. V. Rao and J. A. Owoyale, *J. Heterocyclic Chem.*, 1976, **13**, 1293–1295.
33 Y. Zhang, D. Wang, L. Yang, D. Zhou and J. Zhang, *PLoS One*, 2014, **9**, e105725.
34 A. Carino, F. Moraca, B. Fiorillo, S. Marchianò, V. Sepe, M. Biagioli, C. Finamore, S. Bozza, D. Francisci, E. Distrutti, B. Catalanotti, A. Zampella and S. Fiorucci, *Front. Chem.*, 2020, **8**, 572885.
35 D. Bojadzic, O. Alcazar, J. Chen, S.-T. Chuang, J. M. Condor Capcha, L. A. Shehadeh and P. Buchwald, *ACS Infect. Dis.*, 2021, **7**, 1519–1534.
36 H. G. Toor, D. I. Banerjee, S. Lipsa Rath and S. A. Darji, *Eur. J. Pharmacol.*, 2021, **890**, 173720.
37 C. Zhang, *ACS Omega*, 2022, **7**, 18206–18212.
38 Z. Lin and Y. Will, *Toxicol. Sci.*, 2011, **126**, 114–127.
39 A. Daina, O. Michielin and V. Zoete, *Sci. Rep.*, 2017, **7**, 42717.
40 C. A. Lipinski, F. Lombardo, B. W. Dominy and P. J. Feeney, *Adv. Drug Delivery Rev.*, 2001, **46**, 3–26.
41 C. A. Lipinski, *J. Pharmacol. Toxicol. Methods*, 2000, **44**, 235–249.
42 N. A. Meanwell, *Chem. Res. Toxicol.*, 2011, **24**, 1420–1456.
43 D. F. Veber, S. R. Johnson, H.-Y. Cheng, B. R. Smith, K. W. Ward and K. D. Kopple, *J. Med. Chem.*, 2002, **45**, 2615–2623.
44 L. Guan, H. Yang, Y. Cai, L. Sun, P. Di, W. Li, G. Liu and Y. Tang, *MedChemComm*, 2019, **10**, 148–157.
45 H. Cao, X. Jing, D. Wu and Y. Shi, *Int. J. Food Sci. Nutr.*, 2013, **64**, 437–443.
46 V. Prachayasittikul and V. Prachayasittikul, *EXCLI J.*, 2016, **15**, 113–118.
47 W. J. Geldenhuys, A. S. Mohammad, C. E. Adkins and P. R. Lockman, *Ther. Delivery*, 2015, **6**, 961–971.
48 C. A. Lipinski, F. Lombardo, B. W. Dominy and P. J. Feeney, *Adv. Drug Delivery Rev.*, 2001, **46**, 3–26.
49 Y. C. Martin, *J. Med. Chem.*, 2005, **48**, 3164–3170.
50 J. B. Baell and J. W. M. Nissink, *ACS Chem. Biol.*, 2018, **13**, 36–44.
51 R. Brenk, A. Schipani, D. James, A. Krasowski, I. H. Gilbert, J. Frearson and P. G. Wyatt, *ChemMedChem*, 2008, **3**, 435–444.

